

PPM: Preamble and Postamble-Based Multi-Packet Reception for Green ZigBee Communication

Zhe Wang^{ID}, Student Member, IEEE, Linghe Kong^{ID}, Senior Member, IEEE, Kangjie Xu^{ID}, Guihai Chen, and Liang He^{ID}, Senior Member, IEEE,

Abstract—ZigBee, a low-power wireless communication technology, has been used in various applications, such as smart health/home/buildings. The proliferation of ZigBee-based applications (and thus devices), however, makes the concurrent transmissions—i.e., multiple transmitters send packets to the same receiver at the same time—common in practice, leading to inevitable collisions. Either retranmissions caused by collisions or the collision avoidance mechanism, e.g., CSMA/CA, introduces plenty of energy consumption. To facilitate the green and concurrent transmissions of ZigBee, we design pre/post-amble-based multi-packet reception (PPM), a method that recovers the collided ZigBee messages by exploiting their collision-free chips and the overlapped chips in their pre/post-ambles. We elaborately attach short postamble to standard ZigBee packet by manipulating the ZigBee payload, which can be compatible with standard ZigBee and only introduce negligible energy overhead. We further propose two design enhancements, cross-validation and reference chips calibration, to ensure the accuracy of PPM. Such a collision recovery of PPM reduces the retranmissions caused by collisions and eliminates the energy overhead of CSMA/CA simultaneously, facilitating the realization of green ZigBee. We have prototyped and evaluated PPM with USRP, showing PPM recovers the collided messages with bit-error-rates in the order of 10^{-6} , which is magnitudes lower than state-of-the-art methods. Experimental results show that PPM can achieve packet reception ratio more than 90% and less than 20 retranmissions in a concurrent transmission experiment with 400 packets resulting in negligible packet retranmission cost of energy.

Index Terms—ZigBee, green, collision, decomposition.

I. INTRODUCTION

ZIGBEE [2], a low-power wireless protocol based on the IEEE 802.15.4 standard, has been widely used in applications such as smart home [3] and transportation systems [4],

Manuscript received January 4, 2019; revised March 26, 2019; accepted April 16, 2019. Date of publication April 24, 2019; date of current version August 16, 2019. This work was supported in part by the National Key Research and Development Program of China under Grant 2018YFB1004703, in part by NSFC under Grant 61672349, Grant 61672353, and Grant 61672349, and in part by the Shanghai Key Laboratory of Scalable Computing and Systems at Shanghai Jiao Tong University. This article extends our previous work published in IEEE GLOBECOM'18 [1]. The associate editor coordinating the review of this paper and approving it for publication was E. Ayanoglu. (*Corresponding author: Linghe Kong*)

Z. Wang, L. Kong, K. Xu, and G. Chen are with the Department of Computer Science and Engineering, Shanghai Jiao Tong University, Shanghai 200240, China (e-mail: wang-zhe@sjtu.edu.cn; linghe.kong@sjtu.edu.cn; xkjac04452017@sjtu.edu.cn; chen-gh@sjtu.edu.cn).

L. He is with the Department of Computer Science and Engineering, University of Colorado at Denver, Denver, CO 80217 USA (e-mail: liang.he@ucdenver.edu).

Digital Object Identifier 10.1109/TGCN.2019.2912979

thanks to its short-distance, low-energy, and low-cost features. It is envisioned that ZigBee will draw even more attentions with the further development of Internet of Things (IoT) [5], [15], [19], [36], [37] and cross technology communication (CTC) [6], [16].

The proliferation of ZigBee devices, however, makes the concurrent transmission, i.e., multiple transmitters send packets to the same receiver at the same time in sending the ZigBee messages, common in practice. Standard ZigBee cannot support concurrent transmissions fundamentally, leading to frequently packet retranmissions when collisions happen. Either retranmissions caused by collisions or the collision avoidance mechanism, e.g., Carrier-sense Multiple Access with Collision Avoidance (CSMA/CA), introduces plenty of energy consumption. Standard ZigBee adopts CSMA/CA [7] in its media access control (MAC) layer to avoid collisions, at the cost of additional energy and time consumption for synchronization and channel contention [13], [18]. Existing works analysis wireless CSMA/CA network in details [22]. They try to reduce energy and time consumption by targeted improve the design of CSMA/CA in specific scenarios [23], [24]. Instead of optimizing collision avoidance mechanism, we propose a new green communication paradigm which eliminates additional energy consumption of MAC layer by physical (PHY) layer design. Our design enables multiple ZigBee devices to access channel whenever there are data to be sent without carrier sensing.

In order to realize the alternative functionality of MAC layer, our design should have the ability to recover collided packets. Collision recovery, instead of avoidance, has been demonstrated to be an effective alternative to facilitate ZigBee's concurrent transmission [8], [9]. Collision recovery methods achieve lower power and time consumption compared with standard ZigBee, so long as certain packet reception ratio (PRR) can be achieved. According to the energy consumption of different protocol phases in ZigBee's transmission [13], less than 50% of the total energy is used for transmission and 25% of the energy is spent during CSMA/CA contention as shown in Fig. 1(a). Thus, the energy consumption for retranmissions when collision recovery fails will be less than the persistent overhead of channel contention in standard ZigBee as long as the PRR is larger than 67% for concurrent transmissions without CSMA/CA.

These existing collision recovery methods, however, suffer from accumulated error in packet reception. For example, Fig. 1(b) plots the bit error rate (BER) of mZig [9], a

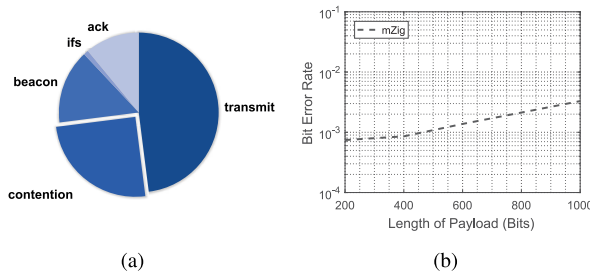


Fig. 1. (a) Breakdown of overhead. (b) Accumulative error of mZig.

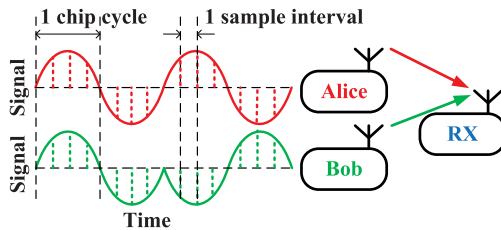
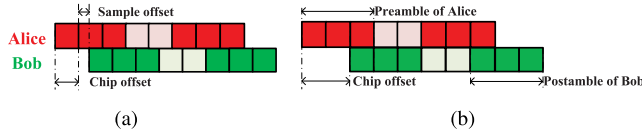


Fig. 2. An example of concurrent transmission with two TXs and one RX.

Fig. 3. Two categories of time offsets: chip offset C_o and sample offset S_o .

state-of-the-art collision recovery method that decomposes collided packets based on the features of ZigBee's physical layer, showing mZig's BER increases significantly with longer packets due to accumulated errors.

To mitigate this deficiency, we design a novel physical layer of ZigBee, called *Pre/Post-amble Based Multi-Packet Reception* (PPM), which achieves ppm-level (i.e., 10^{-6}) BER in recovering the collided messages. PPM attaches short preamble to standard ZigBee packet by manipulating the payload which are therefore compatible with standard ZigBee, and then extracts received signals/samples of single chips representing bit 0 or 1 and the overlap of chips from multiple transmitters (TX) based on the known pre/post-ambles, called *reference chips*, to recover the collided packet by comparison. We further propose two design enhancements to ensure the accuracy of PPM. The first is decoding the collided packets multi-time referring to reference chips of multi-transmitter and cross-validating the decoding result. The second is calibrating the generated reference waveform utilizing correctly decoded collision-free chips or overlapped chips.

Let us use a walk-through example shown in Fig. 2 to explain PPM's core idea: Alice (A) and Bob (B) concurrently send packets to a receiver (RX) and a collision occurs at RX. Because Alice and Bob are not synchronized, time offset usually exists between their packets' arrivals at RX, as shown in Fig. 3. Experimental results in [9] demonstrate over 96% collisions have such time offsets. These time offsets may include

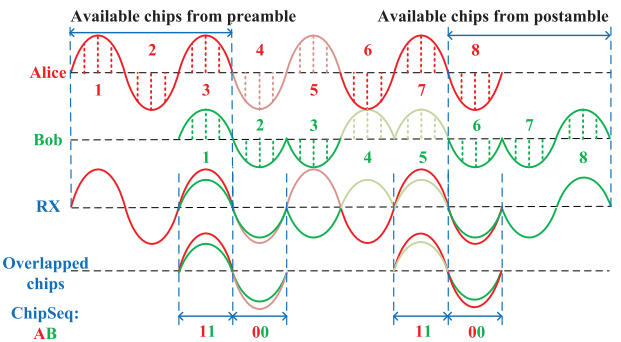


Fig. 4. Decode two-packet collision with only chip offset in PPM.

chip offset, sample offset, or both of them, where the duration of chip offset is of several chip cycles and sample offset consists of several sample intervals as depicted in Fig. 3(a).

PPM's construction of the reference chips can be divided into the following 3 cases.

- 1) If the collision has only chip offset, we can obtain two kinds of information. First, there are several collision-free chips in pre/post-ambles, e.g., the first two chips of A and the last two chips of B in Fig. 4, which can be directly identified. Using these collision-free chips, we can generate the *single reference chips* (\mathbf{R}) representing 0 or 1. Second, some chips in pre/post-amble are overlapped. As there are two transmitters in this example, the overlapped chips have a total number of four possible combinations: 00, 01, 10 and 11. The overlapped chips of these four combinations can be found in the overlapped pre/post-amble as shown in Fig. 4. We can extract *2-overlapped reference chips* (\mathbf{R}^2) by averaging these overlapped chips.
- 2) If the collision has sample offset, we observe that one overlap unit (duration of one chip cycle) involves exactly three chips. For example, a chip of A is overlapped with two partial chips of B as shown in Fig. 5. Denoting the sequence of these three chips as 'BAB' or 'ABA', 'A'/B' represents the current chip values of packet A/B. In Fig. 5, we mark the chip sequence representing the overlap combination as '000' and '111'. Hence, the overlapped chips have totally 8 combinations for A and B, respectively. We can extract these combinations from pre/post-amble as depicted in Fig. 5, named *3-overlapped reference chips* (\mathbf{R}^3).
- 3) If the collision has both chip offset and sample offset, which is the most cases in concurrent transmission, we have both collision-free chips and 3-chip overlaps. Especially, the abstracted \mathbf{R}^3 from the pre/post-amble may be incomplete, i.e., some overlap combinations are not appeared. In this case, we use linear transformation of collision-free chips and abstracted overlaps to generate the missing one, which we will introduce in details in Section III.

With the thus-constructed reference chips, PPM compares the overlapped payload and the reference chips to identify the collision chip-by-chip.

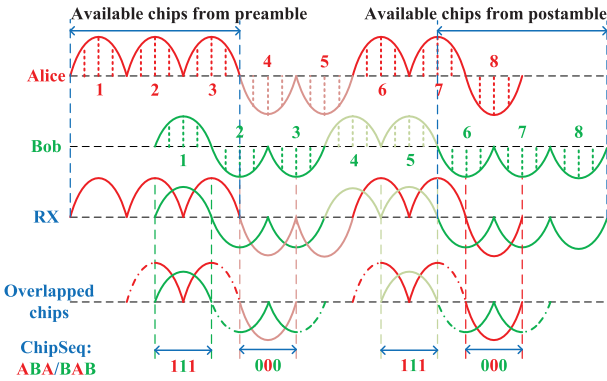


Fig. 5. Decode two-packet collision with chip and sample offsets in PPM.

This paper makes the following major contributions.

- Design of PPM, a novel physical layer technique to decode the collided ZigBee packets without suffering from the accumulative error which can be effortlessly compatible with standard ZigBee.
- Implement and evaluation of PPM with USRPs, showing PPM achieves (i) BER of 10^{-6} , which is 2 magnitudes lower than state-of-the-art solutions, (ii) a *packet reception ratio* (PRR) of 90%, and (iii) less than 20 retransmissions in a concurrent transmission experiment with 400 packets resulting in negligible *packet retransmission cost of energy* (PRC).

The rest part is organized as follows. Section II introduces ZigBee's physical layer and unique features related to our design. Section III designs core of PPM. Section IV shows the experiment configuration and result. Section V presents the related works and Section VI concludes this paper.

II. BACKGROUND

We first review the physical layer of standard ZigBee and introduce ZigBee's unique features related to our design.

A. Physical Layer of Standard ZigBee

The standard ZigBee [2] has three ISM bands: 868.3MHz in Europe, 902-928MHz in America, and 2.4GHz worldwide. Among them, 2.4 GHz ISM band is the most widely used band and its corresponding bit rate is 250kbps. The data frame of ZigBee consists of 3 parts: Synchronization Header (SHR), Physical Layer Header (PHR) and Protocol Service Data Unit (PSDU) as shown in Fig. 8. The 32-bit preamble is a part of SHR which consists of 32 zeros.

Fig. 6 shows the flow graph of ZigBee's transmission: the transmitter (TX) sends bitstream using five procedures and the receiver (RX) receives data with corresponding inverse procedures. Here we mainly focus on the first three processes including spread, modulation and pulse shaping. Firstly, ZigBee adopts Direct Sequence Spread Spectrum (DSSS) as its spreading. In this step, each symbol made up of 4 bits is transformed into 32 chips according to a decided mapping table. Next, ZigBee modulates chips exploiting O-QPSK. As a result, chips in one packet have nearly uniform amplitude. Then pulse

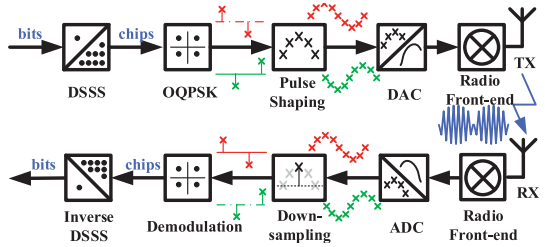


Fig. 6. Physical layer of standard ZigBee.

shaping is performed and all the chips in one packet are shaped as half-sine wave with positive or negative amplitude of the same absolute value.

B. Feature of ZigBee

The standard ZigBee has the following two features that closely relate to our design.

- Preamble: Every ZigBee's frame has a preamble of 32 bits, i.e., 256 decided chips.
- Pulse shaping and modulation: These two components present that chips 0 or 1 in one packet have identical waveforms.

Next we will show more details of our design based on these features.

III. CORE DESIGN OF PPM

In this part, we present PPM design in details.

A. Overview of PPM

1) *Overview*: Based on the above features of ZigBee, we propose the novel Preamble and Postamble based Multi-packet reception (PPM). The main idea of PPM is abstracting reference chips from known data to recover unknown overlapped chips. Leveraging the known pre-/postambles and the detectable time offsets, all combinations of reference chips can be synthesized. Since chips in the same packet are transmitted in short terms, i.e., they meet the same channel state, the overlapped chips can be recognized by comparing reference chips. As a result, we can achieve accurate decoding of collided packets, which reduces retransmission times when collisions happen and corresponding energy consumption. To ensure the high and stable accuracy of PPM and reduce the energy overhead of retransmissions when collision decoding fails, we utilize two iterative mechanisms, cross validation and reference chips calibration, in the decoding process.

The flow chart of PPM is illustrated in Fig. 7. PPM abstracts available known chips from pre- and postamble. After that, reference chips are calculated by averaging known data of the same values. By combining existing overlapped reference chips and single reference chips, sufficient overlapped reference chips can be synthesized. Otherwise, we can seek to other methods for help. After all combinations of reference chips are generated, the collided packets can be decoded precisely by mapping unknown overlapped chips with reference chips since the chip arrays of reference chips are known.

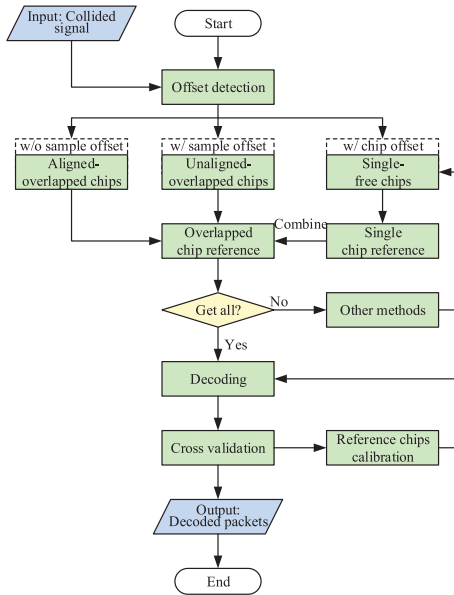


Fig. 7. Flow chart of PPM.

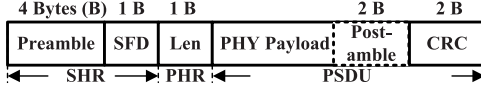


Fig. 8. Packet Structure after Attaching Postamble.

2) *Functionality of Postamble:* The reference chips cannot be synthesized by the standard chips from TXs because the received packet affected by the dynamic channel is usually different from the standard ones. We can only get the known information from the received and collided packet at RX and the known information is limited by short-length preamble.

In order to obtain more known information, we attach 16 bit ‘0’ postamble before the packet CRC field in the transmitter which can be achieved by just manipulating the ZigBee payload as shown in Fig. 8. While we cannot control the CRC field directly, the postamble is attached before CRC field and can be detected utilizing correlation similar as the preamble. The preamble remains unchanged to be compatible with standard ZigBee. As shown in Fig. 9, PPM can cooperate seamlessly with standard ZigBee. In the receiver, we detect the packet collisions according to the correlation results. If collisions happen, PPM can extract reference chips from pre-/post-amble and then decode the collided packets. Otherwise, ZigBee receiver decode the received packet directly and the postamble is discarded in the final frame.

The postamble is attached mainly lies in two aspects. On the one hand, by collecting more collision-free and overlapped chips in pre- and postamble, reference chips can be estimated more accurately. On the other hand, the number of available chips depends on the time offset between collided packets. We simplify the collision model by leaving out the CRC field. We make sure that there are always available chips as reference chips in pre- or postamble by introducing postamble in two-packet collision decoding. As shown in Fig. 10, when the time offset between A and B is less than the duration of preamble,

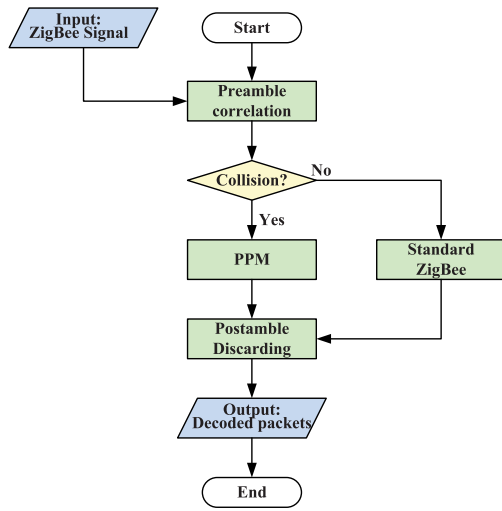


Fig. 9. Compatibility of PPM.

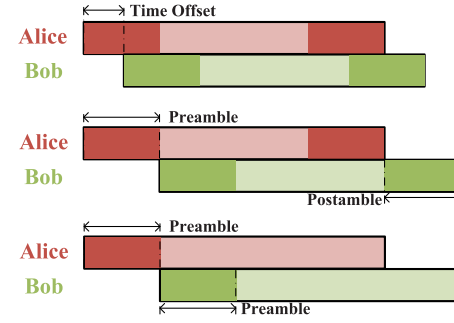


Fig. 10. Two-packet Collision Scenario w/ and w/o (bottom) Postamble.

we have both collision free chips and overlapped chips of A or B as reference. In another case in which the time offset is larger than the duration of preamble, the whole A’s preamble or B’s postamble part is collision free and thus we can also generate all combinations of reference chips based on these collision free chips. On the contrary, there exist none available known chips for packet B if time offset is larger than the length of preamble when postamble is not attached. Fig. 11 show the proportion of two-packet collisions which could be decoded directly with or without postamble. It can be observed that the design of PPM can decode most of the collisions as long as there exists time offsets between two collided packets. Assuming the packet length of 32 bytes, only 12.5% collisions can be decoded when postamble is not attached because only A’s preamble is available if time offsets are larger than the duration of preamble.

In three-packet collision as shown in Fig. 12, there are available collision free chips for at least 2 packets, e.g., A and C, due to the existence of postamble. However, it is possible that B’s pre-/postamble is completely overlapped with the payload of A and C as shown in the bottom of Fig. 12 because of the randomness of time offsets. In this kind of scenario, we only need to decode several chips from pre-/postamble of B as B’s reference chips. We have to decode part of B’s and C’s preamble chips as reference if there exists no postamble. For n-packet collision when $n \geq 3$, we can seek to other method,

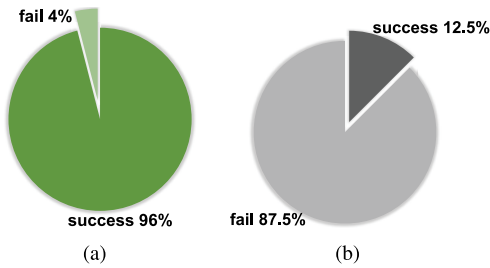


Fig. 11. Proportion of Two-packet Collisions Decoded by the Reference Chips Successfully. (a) w/ Postamble, (b) w/o Postamble.

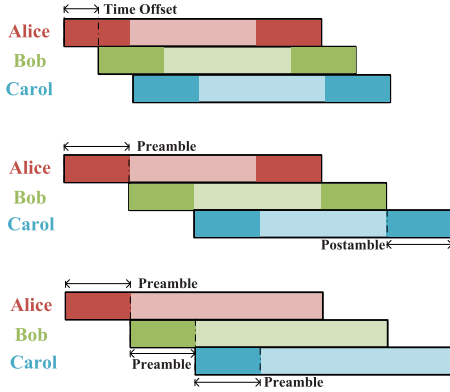


Fig. 12. Three-packet Collision Scenario w and w/o (bottom) Postamble.

e.g., mZig [9] and ZigZag [8], to extract several chips from pre-/postamble for reference chips generation.

3) *Two-Packet Collision Decoding*: To show how PPM decodes collided packets in details, we give two examples of two-packet collision in Fig. 5 and Fig. 4. Time offset between packets from different TXs can be detected and calculated by self-correlation as mentioned in [7], [8]. Time offset is the sum of two parts which are chip offset and sample offset. The number of chips cycles in *chip offset* and the number of sample intervals in *sample offset* is denoted by C_o and S_o respectively. The number of sample intervals in one chip cycle is denoted by λ , which is determined by bandwidth and sampling rate.

Considering two packets from A and B of the same length L in chips, the number of known chips are denoted by $2t$ where t is the length of pre- and postamble. The received chips from A or B in the RX are denoted as $A[i]$ or $B[i]$ respectively, where i is the i -th chip in the packet. Meanwhile, a chip of A or B consists of λ sample points, which can be represented as $A[i][j]$ or $B[i][j]$ where j is the j -th sample in one chip. Next, we will show details about how to extract reference chips utilizing A as an example.

Collision with chip offset: After time offset is detected, available known chips are abstracted from pre- and postamble as shown in Fig. 5 and Fig. 4. When two-packet arrives at RX with chip offset, there are several collision-free chips, e.g., $A[1]$ and $B[8]$. Since waveforms of chips representing the same binary value are identical in one packet, we can calculate the *single reference chips* (\mathbf{R}) representing 0 or 1 by averaging collision-free chips. Denoting the chip value of $A[i]$ as V_i ,

TABLE I
BIT SEQUENCE OF OVERLAP COMBINATION WITH SAMPLE OFFSET

Bob	0	0	0	0	1	1	1	1
Alice	0	0	1	1	0	0	1	1
Bob	0	1	0	1	0	1	0	1
BitSeq	000	001	010	011	100	101	110	111

$\mathbf{R}_A[k]$ can be calculated as follows:

$$\mathbf{R}_A[k][j] = \frac{\sum_{V_i=k} A[i][j]}{\sum_{V_i=k}}, (1 \leq j \leq \lambda). \quad (1)$$

where $k = 0/1$ and $1 \leq i \leq \min(C_o, t)$. More precise estimate of \mathbf{R} can be achieved by averaging the impact of noise, multi-path and other channel factors. Besides, by appending postamble, collision-free chips of B also exist in the packet tail. In Fig. 5, $\mathbf{R}_A[1]$ for A's chip 1 and $\mathbf{R}_B[0]$ for B's chip 0 can be obtained.

Collision with sample offset: When there exists sample offset between packets from two-TX, we observe that in a collision, one chip of A is overlapped with two parts of sequential B's chips as shown in Fig. 3. It is the same for B's overlapped chips. Denoting the result of overlap by a sequence of 'BAB' or 'ABA', each overlapped chip of A or B can be labeled with a specific chip array. In Fig. 5, we can abstract known overlapped chips from pre- and postamble of A and B, e.g., $A[8]$ with label '000' and $B[1]$ with label '111'. After that, 3-overlapped reference chips (\mathbf{R}^3) can be calculated by averaging known overlapped chips of the same chip array. Denoting V_i as the value of the chip array of $A[i]$, \mathbf{R}_A^3 can be computed as follows:

$$\mathbf{R}_A^3[k][j] = \frac{\sum_{V_i=k} A[i][j]}{\sum_{V_i=k}}, (0 \leq k \leq 7, 1 \leq j \leq \lambda). \quad (2)$$

where $C_o + 2 \leq i \leq t$ or $L - t + C_o + 2 \leq i \leq L$. In Fig. 5, $\mathbf{R}_A^3[0]$ and $\mathbf{R}_A^3[6]$ can be estimated by A's overlapped chip $A[8]$, $A[3]$ which are labeled '000', '110'.

For a two-packet collision with sample offset, there are 8 combinations of \mathbf{R}^3 for A and B respectively as shown in Table I. When \mathbf{R}^3 or \mathbf{R} are incomplete, we can combine existing \mathbf{R}^3 and \mathbf{R} together based on the sample offset. \mathbf{R}_A of chip 0 or 1 can be abstracted by subtracting two partial \mathbf{R}_B from existing \mathbf{R}_A^3 as shown in Fig. 13. This procedure can be formulated as follows:

$$\mathbf{R}_A[k[1]][j] = \begin{cases} \mathbf{R}_A^3[k][j] - \mathbf{R}_B[k[0]][l], \\ \quad (1 \leq j \leq S_o, \lambda - S_o + 1 \leq l \leq \lambda); \\ \mathbf{R}_A^3[k][j] - \mathbf{R}_B[k[2]][l], \\ \quad (S_o + 1 \leq j \leq \lambda, 1 \leq l \leq \lambda - S_o). \end{cases} \quad (3)$$

where ' $k[0]k[1]k[2]$ ' denotes the chip array of $\mathbf{R}_A^3[k]$.

Leveraging existing $\mathbf{R}_A^3[0]$ and $\mathbf{R}_B[0]$, $\mathbf{R}_A[0]$ can be obtained as depicted in Fig. 13. And the average value of abstracted \mathbf{R}_A representing the same chip will be calculated as the final result. After that, any combinations of \mathbf{R}_A^3 can be

TABLE II
BIT SEQUENCE OF OVERLAP COMBINATION WITH ONLY CHIP OFFSET

Alice	0	0	1	1
Bob	0	1	0	1
BitSeq	00	01	10	11

generated by the overlay of \mathbf{R}_A and \mathbf{R}_B as follows:

$$\mathbf{R}_A^3[k][j] = \begin{cases} \mathbf{R}_A[k[1]][j] + \mathbf{R}_B[k[0]][l], & (1 \leq j \leq S_o, \lambda - S_o + 1 \leq l \leq \lambda); \\ \mathbf{R}_A[k[1]][j] + \mathbf{R}_B[k[2]][l], & (S_o + 1 \leq j \leq \lambda, 1 \leq l \leq \lambda - S_o). \end{cases} \quad (4)$$

As shown in Fig. 14, unknown $\mathbf{R}_A^3[1]$ can be generated by the overlay of $\mathbf{R}_B[0]$, $\mathbf{R}_A[0]$ and $\mathbf{R}_B[1]$.

Since \mathbf{R}^3 having the same chip sequence is the most similar one with the real overlapped chip as shown in Fig. 5, we can match chip sequence of unknown overlapped chips by known \mathbf{R}^3 . After all combinations of \mathbf{R}^3 are obtained from existing data, we can calculate the root mean square error (RMSE) between unknown overlapped chips $O[i]$ and \mathbf{R}^3 as follows:

$$RMSE(O[i], \mathbf{R}^3[k]) = \sqrt{\frac{\sum_{j=1}^{\lambda} (O[i][j] - \mathbf{R}^3[k][j])^2}{\lambda}}. \quad (5)$$

Based on equation (5), we can get the most similar \mathbf{R}^3 for a given overlapped chip, whose RMSE is the smallest.

Collision without sample offset: When there is no sample offset, we also abstract known collision-free chips according to chip offset and pre- or postamble length. In Fig. 4, all kinds of \mathbf{R} of A and B can be estimated using collision-free chips $A[1]$, $A[2]$ and $B[7]$, $B[8]$. Besides, chips from A and B are aligned since there is no sample offset. We can get 2-overlapped reference chips (\mathbf{R}^2). Each \mathbf{R}^2 can be labeled with a chip array ‘AB’. For a two-packet collision without sample offset, there are 4 kinds of \mathbf{R}^2 totally as shown in Table II. However, not all combinations of \mathbf{R}^2 can be obtained directly and we can only acquire $\mathbf{R}^2[0]$ and $\mathbf{R}^2[3]$ in Fig. 4. Leveraging existing \mathbf{R} and \mathbf{R}^2 , unknown \mathbf{R} can be abstracted as follows:

$$\mathbf{R}_A[k[0]][j] = \mathbf{R}^2[k][j] - \mathbf{R}_B[k[1]][j], (0 \leq j \leq \lambda). \quad (6)$$

where k is the value of $\mathbf{R}^2[k]$ ’s chip array and ‘ $k[0]k[1]$ ’ denotes the corresponding chip array. The rest combinations of \mathbf{R}^2 can be generated by the overlay of \mathbf{R} , which can be formulated as follows:

$$\mathbf{R}^2[k][j] = \mathbf{R}_A[k[0]][j] + \mathbf{R}_B[k[1]][j]. \quad (7)$$

where $0 \leq k \leq 3$ and $1 \leq j \leq \lambda$. On the basis of all combinations of \mathbf{R}^2 , we can match collided packets chip-by-chip. Choosing the \mathbf{R}^2 which has the smallest RMSE for a specific overlapped chip, we can acquire a high accuracy estimation for the whole collision.

Further Improvement of PPM: In a standard ZigBee packet, there are 256 known chips in the preamble. We divide preamble into preamble and postamble of 128 chips in our design.

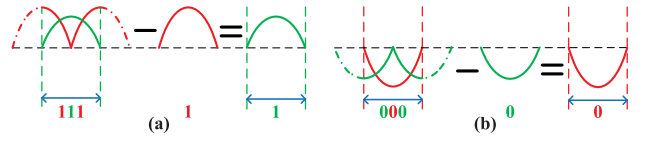


Fig. 13. Obtain the reference waveform of single chip by minus operation between the known overlapped waveform and another single chip. (a) Obtain Bob’s 1 by minusing Alice’s 1s from the overlapped 111. (b) Obtain Alice’s 0 by minusing Bob’s 0s from the overlapped 000.

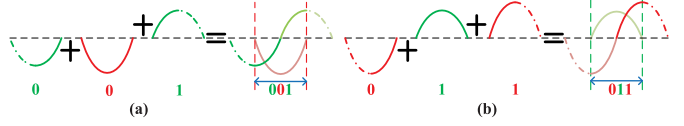


Fig. 14. Generate the reference waveform of overlapped chips by add operation of two known single chips. (a) Bob’s 01 plus Alice’s 0 equals to 001. (b) Alice’s 01 plus Bob’s 1 equals to 011.

Thus, it is of high probability that we can obtain all combinations of $\mathbf{R}^2/\mathbf{R}^3$ and complete \mathbf{R} according to known chips in pre- and postamble, e.g., 4 combinations of \mathbf{R}^2 and 16 combinations of \mathbf{R}^3 for two-packet collision with or without sample offset. Otherwise, by combining available $\mathbf{R}^2/\mathbf{R}^3$ and \mathbf{R} , other combinations of $\mathbf{R}^2/\mathbf{R}^3$ can be generated as mentioned before. However, it is possible that there is no chip offset between multi-packet. Under such circumstance, we can decompose chips of pre- and postamble utilizing other methods, e.g., ZigZag [8] and mZig [9]. Leveraging these known decomposed chips from pre- and postamble, all kinds of \mathbf{R} can be estimated. As a result, any combinations of $\mathbf{R}^2/\mathbf{R}^3$ can be generated by the overlay of \mathbf{R} and the whole packet can be decoded via reference chip comparison.

B. Three-Packet Collision Decoding

In this section, we show that how PPM decodes a three-packet collision.

We give two examples of three-packet collision as shown in Fig. 15 and Fig. 16. Leveraging detected time offset and pre- or postamble length, known collision-free and overlapped chips can be abstracted from pre- and postamble. Based on $A[1]$ and $C[9]$, $\mathbf{R}_A[1]$ for A’s chip 1 and $\mathbf{R}_C[0]$ for C’s chip 0 can be obtained. It is worth noting that five-chip overlaps also exist in pre- or postamble besides three-chip overlaps.

For a three-packet collision with sample offset, we observe that a overlapped chip of A consists of four parts from four different chips of B, C as shown in Fig. 15. Each five-chip overlap can be represented by a 5-bit chip array. By averaging known five-chip overlaps of the same chip array, 5-overlapped reference chips (\mathbf{R}^5) can be acquired and there are 32 combinations of \mathbf{R}^5 for A, B and C respectively. Similarly, unknown \mathbf{R} can be generated by subtracting four partial \mathbf{R} of other chips from existing \mathbf{R}^5 . Besides, \mathbf{R}^5 of five-chip overlaps can be not only formed by the overlay of \mathbf{R} , but also can be generated by overlaying \mathbf{R}^3 of three-chip overlaps with \mathbf{R} . On the basis of all combinations of reference chips, RMSE between the unknown overlapped chips and reference chips can be calculated. By choosing the reference chip which has the smallest RMSE for

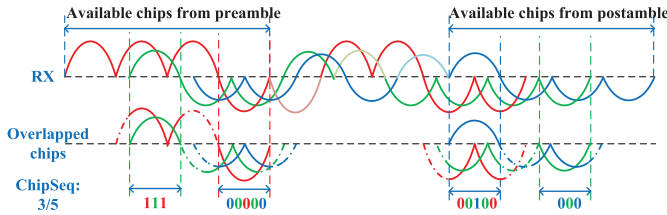


Fig. 15. Decode three-packet collision with chip and sample offsets in PPM.

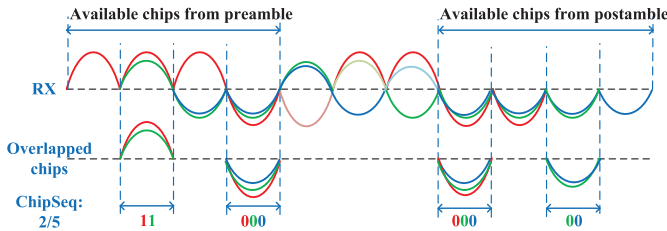


Fig. 16. Decode three-packet collision with only chip offset in PPM.

a specific overlapped chip, the whole collided packet can be decoded accurately.

When there exists no sample offset for a three-packet collision, we also abstract collision-free and overlapped chips. Different from collision with sample offset, each overlapped chip is aligned whose chip sequence can be denoted by a 3-bit array. Partial \mathbf{R}^3 and \mathbf{R} can be calculated based on known chips. Similarly, by combining existing \mathbf{R} and \mathbf{R}^3 , all kinds of reference chips can be generated. After that, the whole collision packet can be decoded by comparing with reference chips.

C. Extending to Multi-Packet Collision

In this subsection, we demonstrate that how to extend PPM to multi-packet collision scenarios.

The flow chart of multi-packet decoding is the same as two-packet scenarios as shown in Fig. 7. After abstracting available chips from pre- and postamble, we can estimate partial reference chips based on known collision-free and overlapped chips. For an n -packet collision, we have to deal with $2, 3, \dots, n$ overlapped chips. After that, we try to abstract all kinds of reference chips by combining known reference chips. If sufficient reference chips cannot be obtained from existing data, we can seek to other methods, e.g., ZigZag [8], mZig [9], for help. We can abstract chip sequence of unknown overlapped chips by comparing known reference chips.

Cross-validation: For an n -packet collision with sample offset, we can decode the collision packet referring to overlapped chips' reference chips of different packets. For example, in three-packet collision with sample offset, we can decode three times referring to reference chips of A, B and C respectively. Thus, each decoding result can be used for cross-validation. As a result, we can achieve a more precise decoding result and the number of retransmissions for multi-packet collision is effectively reduced by our design.

Reference Chips Calibration: To further increase the accuracy of reference chips generation, we calibrate the generated reference chips utilizing correctly decoded collision-free chips

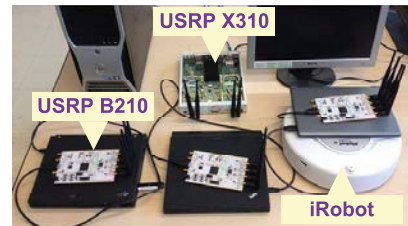


Fig. 17. Our USRP testbed includes three TXs and one RX.

or overlapped chips. Since the reference chips are not exactly identical in the whole collided packet, we dynamically update the reference chip in the decoding process. The correctness of decoded chips can be validated from two aspects, cross-validation and direct sequence spread spectrum. If current decoded chip passes cross-validation and conforms to the DSSS table, we use chip of this collision-free or overlapped chip to calibrate reference chips of single or overlapped chips.

The two enhancement mechanisms are performed iteratively as shown in Fig. 7. First, current chip value is cross-validated according to multi-time decoding results. After that, we verify the correctness of current decoded chip according to cross-validation result and DSSS table. Then, correctly decoded chip will be used to calibrate the reference chips. Last, we decode the following chips based on the updated reference chips. The above processes will be carried out in the whole collision decoding procedure.

IV. EVALUATION

We implement PPM on USRPs and build a 4-node testbed as shown in Fig. 17. We conduct extensive experiments based on this testbed to compare the performance of PPM with existing methods.

A. Experiment Setting

We implement PPM RX in USRP X310, which is connected to a desktop to log the results. We develop PPM TXs in USRP B210s, which are portable and powered by a USB 3.0 port. These TXs are connected to laptops and carried by mobile nodes (i.e., iRobot Roomba). Our experiments are conducted in an office environment with both static and mobile tests.

We compare PPM's performance with the standard ZigBee and mZig. The standard ZigBee is used for unicast, which adopts CSMA/CA to avoid collision and cannot resolve multi-packet collision. mZig [9] resolves the collision using physical layer features but its error will be accumulated with the length of packet. The main purpose of our experiment is to test whether PPM can improve the accuracy of multi-packet collision and reduce retransmission overhead for green communication. We evaluate PPM with three metrics: bit error rate (BER), packet reception ratio (PRR), and packet retransmission cost (PRC) of energy calculated from packet retransmission times (PRT). Since our design focuses on PHY layer collision decomposition, we adopt a simple MAC mechanism in which each unsuccessfully decoded packet only incurs retransmission once. We calculate the packet retransmission cost of energy (PRC) from PRT which can intuitively reflect

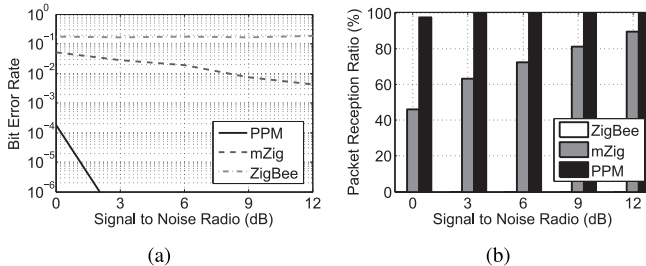


Fig. 18. BER and PRR under different SNRs in two-packet collision.

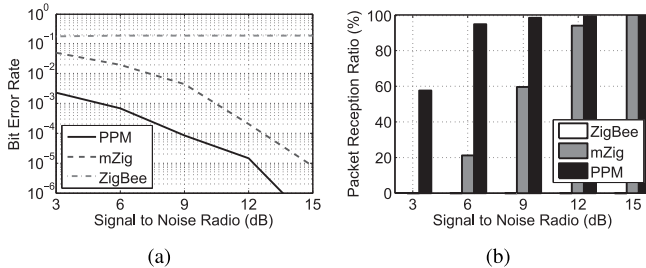


Fig. 19. BER and PRR under different SNRs in three-packet collisions.

the energy efficiency of our design. While all the energy consumption is same for the first transmission, higher PRC means lower energy efficiency as higher total energy is used to transmit the same number of packets.

In our experiment, the number of samples in one chip λ is 32, based on the ADC in USRP. Time offset in a collision is random according to packets' arrivals at TX. We randomly generate equal length packets with the same postamble of 16-bit 0s. The payload is 1000 bits. To estimate the overall performance and impact of different Signal to Noise Radio (SNR), we inject noises and conduct 200 runs for every experiment. In addition, we set a threshold of BER as 10^{-3} , below which we consider that a packet is decoded correctly.

B. Experiment Result

Two-packet collision BER and PRR: Fig. 18 shows BER and PRR comparison of PPM with mZig and ZigBee under different SNRs in two-packet collision decoding. PPM achieves a PPM-level (i.e., 10^{-6}) BER and more than 90% PRR even under very low SNR. As we can see in Fig. 18(a), 18(b), PPM outperforms mZig and ZigBee from both aspects of BER and PRR.

Three-packet collision BER and PRR: Fig. 19 shows performance of PPM and mZig under different SNRs in three-packet collision decoding. We find that the performance of PPM degrades, e.g., BER increases 1 or 2 order of magnitude and PRR decreases 10% on average, compared with two-packet collision scenarios. However, BER of PPM still has 1 or 2 order of magnitude better than mZig. Besides, PRR of PPM can maintain more than 90% when $\text{SNR} \geq 6 \text{ dB}$. This experiment presents that PPM is a general solution for two-three- and multi-packet collision.

BER distribution in two- and three-packet collision: Fig. 20 shows the bit error rate distribution of PPM and mZig in two- and three-packet collision scenarios. The red line show

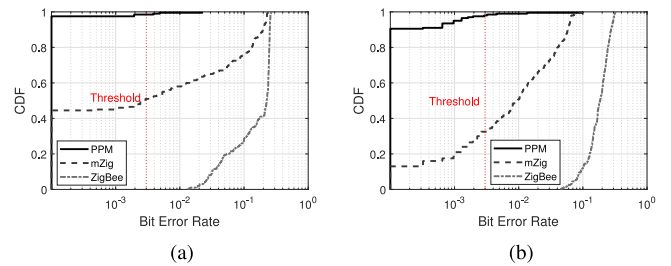


Fig. 20. BER distribution in two- and three-packet collisions. (a) Two-packet collision. (b) Three-packet collision.

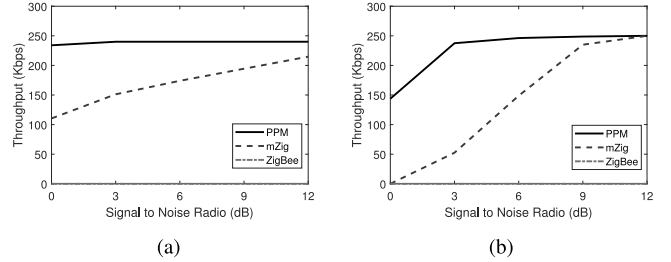


Fig. 21. Throughput under different SNRs in two- and three-packet collisions. (a) Two-packet collision. (b) Three-packet collision.

the industry threshold 3×10^{-3} below which the average bit error rate is acceptable. More than 90% of PPM's BER is lower than the required threshold. While only half of the mZig's decomposed packet can satisfy this requirement, this is because the accumulative error in mZig leads to consecutive error. The performance of PPM outperforms mZig significantly, especially in three-packet collision as shown in Fig. 20(b).

Throughput of two- and three-packet collision: Fig. 21 shows the average throughput of multiple transmitters under difference SNRs in two- and three-packet collision scenarios. We can observe that the throughput of standard ZigBee is 0 since it can not deal with multi-packet collisions fundamentally and the collided packets are abandoned. Throughput of PPM outperforms mZig for 3 \times under severe noise environment. The performance of PPM is also stable compared with mZig which demonstrates its powerful anti-noise ability.

PRT of two- and three-packet collision: Fig. 22 shows the PRT needed for 200 transmissions in two and three packets collision scenarios. For two-packet collision, the PRT of PPM is less than 20 as shown in Fig. 22(a). It can be observed that the performance of mZig degrades a lot in three-packet collisions in Fig. 22(b), this can be well explained that the accumulated error is more severe in three-packet collision decoding.

PRC of two- and three-packet collision: Fig. 23 shows the PRC of 200 transmissions in two and three packets collision scenarios. Since the power consumption of USRP devices cannot be evaluated directly, we estimate the retransmissions energy cost according to the energy consumption per bit result from existing works. Experiment results in [13] give the average energy cost per bit whose value is around $1.5 \cdot 10^{-7} \text{ J/bit}$ under 123 bytes payload. For two-packet collision, the PRT of PPM is less than 20 resulting in less than 1.6 mJ total retransmission energy consumption as shown in Fig. 23(a). In

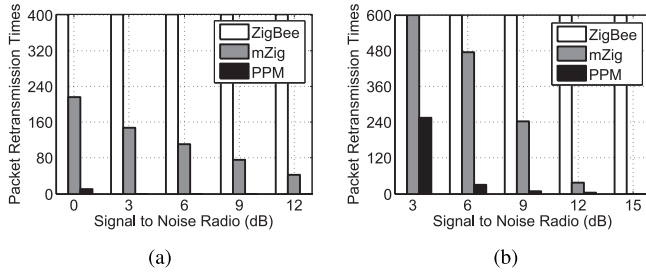


Fig. 22. PRT under different SNRs in two- and three-packet collision. (a) Two-packet collision. (b) Three-packet collision.

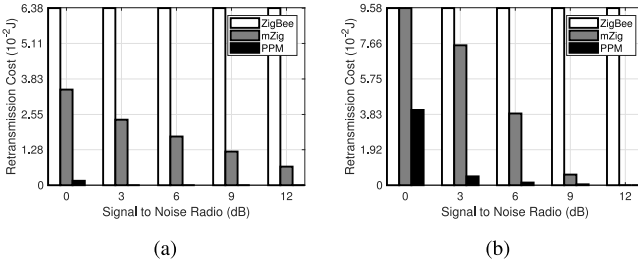


Fig. 23. PRC under different SNRs in two- and three-packet collision to indicate the energy saving. (a) Two-packet collision. (b) Three-packet collision.

three-packet collision, the PRC of PPM still has a huge gap with that of mZig and standard ZigBee as shown in Fig. 23(b).

Evaluation Summary: According to the experimental result, we observe that PPM accurately decodes multi-packet collision and reduces the energy consumption for retransmissions. Different from existing methods, e.g., mZig [9] and ZigZag [8], PPM decouples current chip or chunk from previous ones and decoding each chip or chunk independently without cumulative error. From the collision resolution side, PPM outperforms the advanced mZig in terms of BER and PRR, usually one or two order of magnitude lower than mZig in BER. From the green communication side, PPM can maintain high PRR and low PRT in most cases. By reducing PRT, PPM reduces the energy consumption due to retransmissions significantly.

V. RELATED WORK

Collision is inevitable in concurrent transmissions and there are a lot of studies aiming at solving this problem. Existing research wants to deal with collision problem from different aspects and achieve green communication in concurrent transmissions, which can be roughly divided into two types.

CSMA/CA [7] is a typical example of collision avoidance. However, CSMA/CA is unavailable in hidden terminal scenarios. Besides, CSMA/CA will lead to delay because of exponential backoff algorithm and retransmission when collision happens [11], [18]. Apart from retransmission, channel contentions in CSMA/CA are another major source of extra energy overhead [13]. As a complementary strategy of CSMA/CA, RTS-CTS [10] is proposed to deal with hidden station problem based on handshake. However, RTS/CTS CSMA/CA takes additional channel and power overhead for which it is not recommended in wireless networks [12]. Existing methods try

to reduce power consumption by optimizing the CSMA/CA mechanism [14], [17]. Rafael and Leonard give detailed analysis of wireless CSMA/CA networks [22]. Optimization of IEEE 1901 MAC for power-line networks is presented in [23] which improves network performance without knowing the number of stations. Yang *et al.* reduce the collision time and contention delay in wireless full-duplex network by specific MAC design [24]. A novel MAC protocol for ARQ-based cooperative wireless sensor networks is proposed in [34] to achieve better energy efficiency. By exploiting idle devices as relays and the benefits of network coding (NC), an adaptive cooperative NC-based MAC (ACNC-MAC) protocol is proposed in [33] for the D2D data exchange. However, all these MAC optimizations are based on CSMA/CA mechanism and therefore cannot avoid energy overhead for carrier sensing and channel contention.

Apart from MAC layer optimization, recent works realize green communication from the perspective of utilizing ambient energy or signals in the air. On the one hand, wireless communication devices can harvest energy from ambient light source or wireless signals to support long term operation. Reference [29] gives an overview of the past and recent developments about the energy harvesting transmission schemes, analysis challenges and problems in existing works and give several possible future research orientations. Reference [30] presents a mobile-edge computing system with energy harvesting devices to offload intensive computation into green mobile devices. Reference [31] proposes a new wireless energy harvesting protocol in cognitive relay networks and analysis the trade off between interference from primary user transmitters and the benefits of harvesting energy from primary transmitters. The performance of communication in dense networks with wireless energy harvesting (WEH)-enabled sensor nodes is studied under direct and cooperative communication scenarios in [35]. On the other hand, many works have been done to implement backscatter communication in passive devices which are incapable of generating high frequency carrier. Thus, backscatter communication can save plenty of energy without generating energy-hungry carrier. PLoRa [25] realize long-range wireless connectivity for battery less IoT devices by backscattering and harvesting energy from ambient LoRa signals. BackFi [26] makes use of ambient WiFi signal to enable communication between low power IoT sensor and WiFi APs. Inter-technology backscatter [27] implements cross-technology communication by backscattering ambient wireless signals. Parallel backscatter [28] decodes the collided backscatter signals which cannot be easily distinguishable in parallel. FM backscatter [32] generates commodity FM receiver compatible information by backscattering ambient FM signals, which enables large-scale connectivities in outdoor environments.

Instead of optimizing collision avoidance mechanism and utilizing ambient wireless signal, we propose a new green communication paradigm which eliminates additional energy consumption of MAC layer by PHY layer collision decoding. The state-of-the-art method, e.g., mZig [9], ZigZag [8] try to address collision by decomposing collided packet. ZigZag [8] utilizes the different time offsets between packet

retransmissions. Thus, the ZigZag's throughput is limited. mZig [9] makes use of ZigBee's waveform and amplitude to decompose collision from header to tail. However, mZig falls into high accumulative error and has poor performance under inferior channel conditions. Even though there exist some limitations, collision resolution strategy can reduce energy consumption by eliminating the overhead of CSMA/CA and decreasing retransmissions.

Compared with mZig, PPM can achieve higher decoding accuracy which further reduces the number of retransmissions. As long as there exist known chips in preamble or postamble and the base band signal is almost identical, PPM can be used for collision decoding and green communication in ZigBee and other wireless technologies. Furthermore, PPM can take advantage of mZig or ZigZag as a complementary method for collision resolution.

VI. CONCLUSION

We present PPM, a physical layer design for collision recovery and green transmission in ZigBee. Leveraging known preamble and attached postamble, PPM can resolve multi-packet collisions without accumulative error by comparing reference chips generated from collided packets. Thus, PPM can decode collided packets with a relatively high accuracy which reduces energy consumption of CSMA/CA contention and packet retransmissions simultaneously. Experiment results based on USRP testbed show that PPM can achieve ppm-level BER (i.e., 10^{-6}), which is superior compared with the-state-of-art method, e.g., mZig, and standard ZigBee.

PPM has been implemented in ZigBee but not limited to ZigBee. As long as the reference chips can be obtained from overlapped packets, we can extend PPM to other wireless technologies' accurate and green collision recovery, e.g., Bluetooth Low Energy (BLE).

REFERENCES

- [1] Z. Wang, L. Kong, G. Chen, and L. He "PPM: Preamble and postamble based multi-packet reception for green ZigBee communication," in *Proc. IEEE GLOBECOM*, 2018, pp. 1–6.
- [2] P. Baronti, P. Pillai, V. Chook, S. Chessa, A. Gotta, and Y. Hu, "Wireless sensor networks: A survey on the state of the art and the 802.15.4 and ZigBee standards," *Comput. Commun.*, vol. 30, no. 7, pp. 1655–1695, May 2007.
- [3] S. D. T. Kelly, N. K. Suryadevara, and S. C. Mukhopadhyay, "Towards the implementation of IoT for environmental condition monitoring in homes," *IEEE Sensors J.*, vol. 13, no. 10, pp. 3846–3853, Oct. 2013.
- [4] R. Sundar, S. Hebbar, and V. Golla, "Implementing intelligent traffic control system for congestion control, ambulance clearance, and stolen vehicle detection," *IEEE Sensors J.*, vol. 15, no. 2, pp. 1109–1113, Feb. 2015.
- [5] E. Ronen, A. Shamir, A.-O. Weingarten, and C. O'Flynn, "IoT goes nuclear: Creating a ZigBee chain reaction," in *Proc. IEEE Symp. Security Privacy*, 2017, pp. 195–212.
- [6] Z. Li and T. He, "WEBee: Physical-layer cross-technology communication via emulation," in *Proc. ACM MOBICOM*, 2017, pp. 2–14.
- [7] L. Kleinrock and F. Tobagi, "Packet switching in radio channels: Part I—Carrier sense multiple-access modes and their throughput-delay characteristics," *IEEE Trans. Commun.*, vol. COM-23, no. 12, pp. 1400–1416, Dec. 1975.
- [8] S. Gollakota and D. Katabi, "ZigZag decoding: Combating hidden terminals in wireless networks," in *Proc. ACM SIGCOMM*, 2008, pp. 159–170.
- [9] L. Kong and X. Liu, "mZig: Enabling multi-packet reception in ZigBee," in *Proc. ACM MOBICOM*, 2015, pp. 552–565.
- [10] F. Tobagi and L. Kleinrock, "Packet switching in radio channels: Part II—The hidden terminal problem in carrier sense multiple-access and the busy-tone solution," *IEEE Trans. Commun.*, vol. COM-23, no. 12, pp. 1417–1433, Dec. 1975.
- [11] E. Ziouva and T. Antonopoulos, "CSMA/CA performance under high traffic conditions: Throughput and delay analysis," *Comput. Commun.*, vol. 25, no. 3, pp. 313–321, 2002.
- [12] J. L. Sobrinho, R. de Haan, and J. M. Brazio, "Why RTS-CTS is not your ideal wireless LAN multiple access protocol," in *Proc. IEEE WCNC*, 2005, pp. 81–87.
- [13] B. Bougard, F. Catthoor, D. C. Daly, A. Chandrakasan, and W. Dehaene, "Energy efficiency of the IEEE 802.15.4 standard in dense wireless microsensor networks: Modeling and improvement perspectives," in *Proc. IEEE DATE*, 2005, pp. 196–201.
- [14] Y. Zhang and F. Shu, "Packet size optimization for goodput and energy efficiency enhancement in slotted IEEE 802.15.4 networks," in *Proc. IEEE WCNC*, 2009, pp. 1–6.
- [15] B. Nour, K. Sharif, F. Li, and H. Moungla, "A distributed ICN-based IoT network architecture: An ambient assisted living application case study," in *Proc. IEEE GLOBECOM*, 2017, pp. 1–6.
- [16] S. M. Kim and T. He, "Freebee: Cross-technology communication via free side-channel," in *Proc. ACM MOBICOM*, 2015, pp. 317–330.
- [17] J. Kwak, C.-H. Lee, and D. Y. Eun, "A high-order Markov-chain-based scheduling algorithm for low delay in CSMA networks," *IEEE/ACM Trans. Netw.*, vol. 24, no. 4, pp. 2278–2290, Aug. 2016.
- [18] W. Du, J. C. Liando, H. Zhang, and M. Li, "When pipelines meet fountain: Fast data dissemination in wireless sensor networks," in *Proc. ACM SenSys*, 2015, pp. 365–378.
- [19] Z. Zhou, F. Xiong, C. Xu, Y. He, and S. Mumtaz, "Energy-efficient vehicular heterogeneous networks for green cities," *IEEE Trans. Ind. Informat.*, vol. 14, no. 4, pp. 1522–1531, Apr. 2018.
- [20] Z. Zhou *et al.*, "Energy-efficient stable matching for resource allocation in energy harvesting-based device-to-device communications," *IEEE Access*, vol. 5, pp. 15184–15196, 2017.
- [21] C. Xu *et al.*, "Two-stage matching for energy-efficient resource management in D2D cooperative relay communications," in *Proc. IEEE GLOBECOM*, 2017, pp. 1–6.
- [22] R. Laufer and L. Kleinrock, "The capacity of wireless CSMA/CA networks," *IEEE/ACM Trans. Netw.*, vol. 24, no. 3, pp. 1518–1532, Jun. 2016.
- [23] C. Vlachou, A. Banchs, P. Salvador, J. Herzen, and P. Thiran, "Analysis and enhancement of CSMA/CA with deferral in power-line communications," *IEEE J. Sel. Areas Commun.*, vol. 34, no. 7, pp. 1978–1991, Jul. 2016.
- [24] J. Yang, L. Feng, G. Li, S. Yao, and H. Liang, "Reducing collision time and contention delay for wireless full-duplex," in *Proc. IEEE SmartIoT*, 2018, pp. 235–239.
- [25] Y. Peng *et al.*, "PLoRa: A passive long-range data network from ambient LoRa transmissions," in *Proc. ACM SIGCOMM*, 2018, pp. 147–160.
- [26] D. Bharadia, K. R. Joshi, M. Kotaru, and S. Katti, "BackFi: High throughput WiFi backscatter," in *Proc. ACM SIGCOMM*, 2015, pp. 283–296.
- [27] V. Iyer, V. Talla, B. Kellogg, S. Gollakota, and J. Smith, "Inter-technology backscatter: Towards Internet connectivity for implanted devices," in *Proc. ACM SIGCOMM*, 2016, pp. 356–369.
- [28] M. Jin, Y. He, X. Meng, D. Fang, and X. Chen, "Parallel backscatter in the wild: When burstiness and randomness play with you," in *Proc. ACM MOBICOM*, 2018, pp. 471–485.
- [29] M.-L. Ku, W. Li, Y. Chen, and K. J. R. Liu, "Advances in energy harvesting communications: Past, present, and future challenges," *IEEE Commun. Surveys Tuts.*, vol. 18, no. 2, pp. 1384–1412, 2nd Quart., 2016.
- [30] Y. Mao, J. Zhang, and K. B. Letaief, "Dynamic computation offloading for mobile-edge computing with energy harvesting devices," *IEEE J. Sel. Areas Commun.*, vol. 34, no. 12, pp. 3590–3605, Dec. 2016.
- [31] Y. Liu, S. A. Mousavifar, Y. Deng, C. Leung, and M. Elkashlan, "Wireless energy harvesting in a cognitive relay network," *IEEE Trans. Wireless Commun.*, vol. 15, no. 4, pp. 2498–2508, Apr. 2016.
- [32] A. Wang, V. Iyer, V. Talla, J. R. Smith, and S. Gollakota, "FM backscatter: Enabling connected cities and smart fabrics," in *Proc. USENIX NSDI*, 2017, pp. 243–258.
- [33] E. Datsika, A. Antonopoulos, N. Zorba, and C. Verikoukis, "Cross-network performance analysis of network coding aided cooperative outband D2D communications," *IEEE Trans. Wireless Commun.*, vol. 16, no. 5, pp. 3176–3188, May 2017.
- [34] A. Antonopoulos and C. Verikoukis, "Network-coding-based cooperative ARQ medium access control protocol for wireless sensor networks," *Int. J. Distrib. Sensor Netw.*, vol. 8, no. 1, pp. 601–621, 2011.

- [35] P.-V. Mekikis *et al.*, “Information exchange in randomly deployed dense WSNs with wireless energy harvesting capabilities,” *IEEE Trans. Wireless Commun.*, vol. 15, no. 4, pp. 3008–3018, Apr. 2016.
- [36] J. Wu, M. Dong, K. Ota, J. Li, and Z. Guan, “Big data analysis-based secure cluster management for optimized control plane in software-defined networks,” *IEEE Trans. Netw. Service Manag.*, vol. 15, no. 1, pp. 27–38, Mar. 2018.
- [37] J. Wu, M. Dong, K. Ota, J. Li, and Z. Guan, “FCSS: Fog computing based content-aware filtering for security services in information centric social networks,” *IEEE Trans. Emerg. Topics Comput.*, to be published.



Zhe Wang received the bachelor’s degree from Shanghai University in 2017. He is currently pursuing the Ph.D. degree with the Department of Computer Science, Shanghai Jiao Tong University. His research interests include Internet of Things and wireless networks.



Kangjie Xu is currently an undergraduate student with the Department of Computer Science, Shanghai Jiao Tong University. His research interests include wireless networks, deep learning, and security.



Guanghai Chen received the B.S. degree from Nanjing University in 1984, the M.E. degree from Southeast University in 1987, and the Ph.D. degree from the University of Hong Kong in 1997. He is a Distinguished Professor with Shanghai Jiao Tong University, China. He had been invited as a Visiting Professor by many universities, including the Kyushu Institute of Technology, Japan, in 1998; the University of Queensland, Australia, in 2000; and Wayne State University, USA, from 2001 to 2003. He has a wide range of research interests with a focus on sensor network, peer-to-peer computing, high performance computer architecture, and combinatorics.



Linghe Kong (S’09–M’13–SM’18) received the B.Eng. degree in automation from Xidian University in 2005, the master’s degree in telecommunication from TELECOM SudParis in 2007, and the Ph.D. degree in computer science from Shanghai Jiao Tong University in 2012. He was a Post-Doctoral Researcher with Columbia University, McGill University, and the Singapore University of Technology and Design. He is currently a Research Professor with the Department of Computer Science and Engineering, Shanghai Jiao Tong University. His research interests include wireless networks, big data, mobile computing, and Internet of Things.



Liang He (S’09–M’12–SM’17) received the B.Eng. degree from Tianjin University, China, in 2006 and the Ph.D. degree from Nankai University, China, in 2011. He was a Research Fellow with the University of Michigan at Ann Arbor, MI, USA, a Research Scientist with the Singapore University of Technology and Design, Singapore, and a Research Assistant with the University of Victoria, Canada. He is currently an Assistant Professor with the University of Colorado Denver. His research mainly focuses on cyber-physical systems, Internet of Things, and mobile computing. He was a recipient of the Best Paper Awards of IEEE WCSP’11, IEEE GLOBECOM’11, and QShine’15, and the Best Paper Candidate of IEEE GLOBECOM’14.